

ANALYSIS FOR STEADY PROPAGATION OF A GENERIC RAM ACCELERATOR/OBLIQUE DETONATION WAVE ENGINE CONFIGURATION*

Joseph M. Powers[†] David R. Fulton[‡] Keith A. Gonthier[§] and Matthew J. Grismer[¶]

Department of Aerospace and Mechanical Engineering,
University of Notre Dame,
Notre Dame, Indiana 46556-5637.

Abstract

This study describes a methodology and gives analyses to determine the steady propagation speed of a projectile fired into a gaseous mixture of fuel and oxidizer. For tractability, the steady supersonic flow of an inviscid calorically perfect ideal reacting gas with high activation energy over a symmetric double wedge, unconfined by a cowl, is considered. Propagation speeds are found which give rise to shocks of such strength which induce a reaction zone to be in a region which allows the combustion-induced thrust to balance the wave drag. For a fixed heat release greater than a critical value, two steady propagation speeds are predicted. The solution at the higher Mach number is stable to quasi-static perturbations while the solution at the lower Mach number is unstable. This methodology can be applied to analyze devices which have more complex geometries such as the ram accelerator or oblique detonation wave engine. This paper gives both a simple proof of concept analysis based on Rankine-Hugoniot jump conditions and a detailed numerical analysis of the governing partial differential equations. The simple analysis and numerical analysis are shown to be in qualitative agreement.

Introduction

It is possible to employ oblique shock waves to induce combustion to generate thrust. Recent discussion has been motivated by the ram accelerator, which has been used to propel projectiles to high speeds, and the oblique detonation wave engine (ODWE), which has been proposed to propel the National Aerospace Plane (NASP). For such devices, it

is of fundamental importance to have a theory which can predict a steady propagation speed. The numerical analyses of Brackett and Bogdanoff¹ and Yungster and Bruckner², which consider geometries and material properties similar to potential operating conditions for $H_2 - O_2$ systems, and Rankine-Hugoniot (RH) analysis of Powers and Gonthier³, which considers highly idealized systems in order to retain analytic tractability, predict such speeds in the approximate range 5,000 – 10,000 m/s .

In this paper we present a review, describe a general methodology for determining the steady propagation speed of either ram accelerator projectiles or ODWE-powered aerospace planes, present a simple model problem used to illustrate the methodology, describe standard RH conditions used to evaluate surface forces, develop an estimate of the induction zone length based upon thermal explosion theory, give our results from RH analysis, and compare these to our numerical predictions. Much of the discussion and analysis was first given in Ref. 3; the new contribution of the present paper is the qualitative verification of the earlier analysis by detailed numerical solution of the governing partial differential equations.

Review

The ram accelerator (see Fig. 1) was first tested by Hertzberg, *et al.*^{4,5}. In this application, a high speed projectile is fired at high velocity from a light gas gun into a tube filled with an unreacted mixture of combustible gases. Hertzberg, *et al.*⁵ observed that upon entering a 16 m length, 38 mm bore tube filled in its first three stages with varying combinations of CH_4 , O_2 , N_2 , and He at a pressure of 31 bar and in its final stage with $0.9C_2H_4 + 3O_2 + 5CO_2$ at a pressure of 16 bar , that a shock-induced combustion process accelerated a 70 g projectile from an initial velocity of near 1,200 m/s to a velocity of 2,475 m/s (corresponding to a Mach number, $M = 8.4$) at the end of

*Copyright © American Institute of Aeronautics and Astronautics, Inc., 1993. All rights reserved.

[†]Assistant Professor, Member AIAA.

[‡]Undergraduate Student, Member AIAA.

[§]Graduate Assistant, Member AIAA.

[¶]Graduate Assistant, Member AIAA.

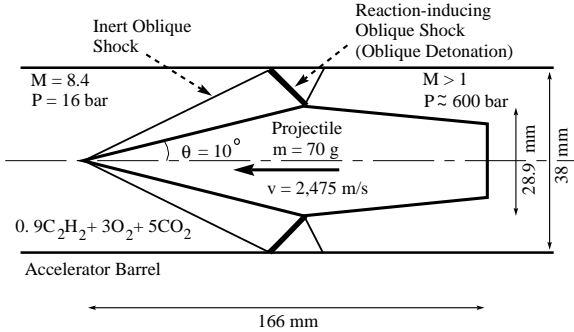


Figure 1: Schematic of ram accelerator, adopted from Hertzberg, *et al.*⁵

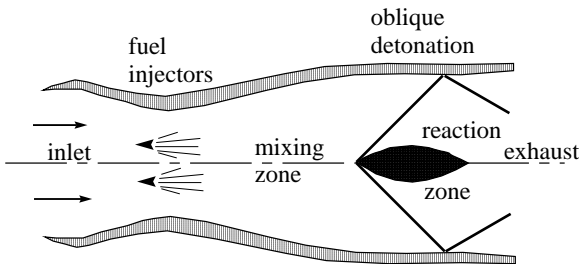


Figure 2: Envisioned oblique detonation wave engine, adopted from Dunlap, *et al.*⁶

the tube, at which location it was still accelerating. Downstream pressures in the neighborhood of 600 *bar* were measured. The diameter of the main body of the projectile was 28.9 *mm*. Its length was 166 *mm* and the leading edge conical half-angle $\theta = 10^\circ$. Four stabilizing fins (not shown) of diameter 38 *mm* were a part of the aft-body. A portion of the oblique shock train is sketched in Fig. 1; the various expansion fans and wave interactions are not included. Figure 1 depicts the first reflected shock triggering significant chemical reaction; the temperature-sensitive reaction would be associated with the lead shock for faster projectile speeds, and with a downstream shock for slower speeds. For even slower speeds, the reaction would be downstream of the projectile. It was suggested that such a device can be scaled for direct launch to orbit, for hypervelocity impact studies, and for a hypersonic test facility.

Another relevant propulsion device is the proposed oblique detonation wave engine (ODWE). The idea of using an ODWE for supersonic combustion for a high-speed plane has existed for decades (*e.g.* Dunlap, *et al.*⁶). The hypothesized operation is as follows (see Fig. 2, adopted from Dunlap, *et al.*). Supersonic air enters the inlet. On-board fuel is injected downstream which mixes with the air without signifi-

cant reaction. The mixture then encounters a downstream wedge. The oblique shock associated with the wedge compresses and ignites the mixture, generating a propulsive force. Relative to conventional air-breathing engines with subsonic combustion, Dunlap, *et al.* cite the ODWE's advantages as 1) simpler supersonic inlet diffuser design since the inherently supersonic oblique detonation does not require deceleration to a subsonic state, 2) reduced total pressure losses, 3) shorter combustion chamber length, 4) no ignition device other than the wedge, and 5) faster flight velocities. Cited concerns are 1) the lack of static thrust, 2) uncertainty as to whether mixing lengths are practical, and 3) uncertainty with regards to the process's stability.

Methodology and Model Problem

Most recent theoretical studies related to ram accelerators and ODWE's⁷⁻¹⁷ have not given analysis to determine a steady propagation speed. Typically these studies treat the related problem of flow with a fixed incoming Mach number over a fixed geometry and concentrate on discussing the features of the resulting flow field. Only a small number of incoming Mach numbers are studied. The problems posed are physical in the sense that one could envision an experiment in which the projectile is fixed in a wind tunnel in which the incoming Mach number is controllable. Such an approach, however, yields little about what the steady speed of a freely propagating vehicle should be.

Here we present a general theoretical approach to predict the steady speed. One first selects a mathematical model for the fluid and a representative geometry. The model equations are studied in the reference frame in which the projectile is stationary; thus, the incoming flow velocity, which is the steady propagation speed, is thought of as an adjustable parameter at this stage. For a given incoming velocity, solution of the model equations leads to a stress distribution on the projectile surface which may or may not result in a net force on the projectile. Should the particular incoming velocity lead to zero net force on the projectile, that velocity is a candidate for a steady propagation speed. The quasi-static stability of the candidate solutions is easily determined. Should a perturbation in the incoming velocity lead to a net force which tends to restore the projectile to its speed at which there is zero net force, the solution is stable in a quasi-static sense (we call such solutions quasi-stable); otherwise the solution is unstable. A further step, not considered here, is to account for the inertia of the projectile and surrounding fluid so as to determine the dynamic stability.

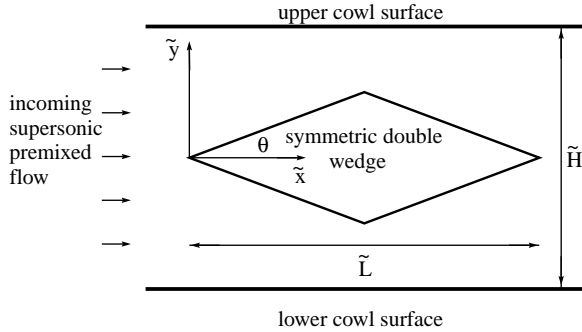


Figure 3: Schematic of generic configuration

We illustrate this methodology through the use of a model problem which is related to the ram accelerator and ODWE. For tractability, we consider an idealized model and geometry which retain the essential physics of the real devices. The geometry, shown in Fig. 3, is a symmetric double wedge with half angle θ and length \tilde{L} . Two cowl surfaces are placed symmetrically about the wedge and are separated by height \tilde{H} . The depth of the double wedge and cowl is taken to be infinite and the flow is assumed to have no variation in this direction. The Cartesian coordinate system, with its origin at the leading edge and with the \tilde{x} axis aligned with the incoming flow is also indicated. It is appropriate to think of a ram accelerator as the axisymmetric analog of Fig. 3 in which the projectile moves while the cowl is stationary; likewise, an aerospace plane powered by an ODWE can be thought of as the axisymmetric analog of Fig. 3 in which the cowl moves with the wedge. In both scenarios one must assume that the incoming fuel and oxidizer are completely mixed; in actuality this is more appropriate for the ram accelerator than the ODWE.

Analysis of the geometry of Fig. 3 leads in general to a complicated interaction of shocks, rarefactions, and combustion processes as the flow propagates between the projectile and cowl surface. To further simplify, we only consider the limit $\tilde{H} \rightarrow \infty$, Fig. 4. Consequently, our geometry shares only a rudimentary resemblance to actual devices, but has the advantage of being amenable to simple analysis.

Again for tractability, the flow model employed also has only a rudimentary resemblance to commonly used models for real devices. We consider a calorically perfect ideal reacting gas with one-step irreversible Arrhenius kinetics; the reactants and products are taken to have the same molecular weights and material properties. In the limit of high activation energy the flow can be broken into discrete regions linked by *RH* jump conditions as shown in Fig. 4. The ambient fluid in Region 0 encounters an

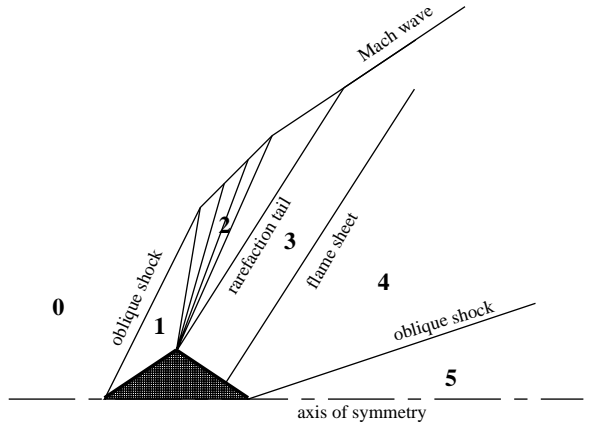


Figure 4: Detailed schematic for $\tilde{H} \rightarrow \infty$

attached oblique shock at the leading edge. No appreciable reaction occurs within the shock or in Region 1, near the front face. The flow is turned through a centered Prandtl-Meyer expansion in Region 2 till it attains a velocity parallel to the lee wedge surface in Region 3. We assume *ad hoc* that the reaction occurs in a flame sheet which is perpendicular to the lee surface. The location of this flame sheet is estimated by an induction zone length based upon thermal explosion theory and is related to the incoming Mach number and kinetic parameters. A *RH* deflagration analysis gives the flow variables in Region 4 based upon values in Region 3 and the heat released in the flame sheet. The flow passes through a final oblique shock to Region 5 where it attains a velocity with only an \tilde{x} component. Away from the high activation energy limit, a numerical analysis can predict the flow and eliminate the need for *ad hoc* assumptions. The net force is then determined by integrating the pressure over the entire surface area.

Model Equations

The model equations are taken to be the unsteady Euler equations and species evolution equation for a reactive calorically perfect ideal gas. These are expressed in dimensionless form below:

$$\frac{d\rho}{dt} + \rho \frac{\partial v_i}{\partial x_i} = 0, \quad (1)$$

$$\frac{dv_i}{dt} + \frac{1}{\rho} \frac{\partial P}{\partial x_i} = 0, \quad (2)$$

$$\frac{dP}{dt} - \gamma \frac{P}{\rho} \frac{d\rho}{dt} = (\gamma - 1) \rho \kappa q (1 - \lambda) \exp\left(\frac{-\Theta}{T}\right), \quad (3)$$

$$\frac{d\lambda}{dt} = \kappa (1 - \lambda) \exp\left(\frac{-\Theta}{T}\right), \quad (4)$$

$$e = \frac{1}{\gamma - 1} \frac{P}{\rho} - \lambda q, \quad (5)$$

$$P = \rho T. \quad (6)$$

The independent variables in Eqs. (1–6) are the density ρ , the Cartesian velocity component v_i , the pressure P , the temperature T , the internal energy e , and the reaction progress variable λ . The dependent variables are time t and the Cartesian position coordinate x_i . The dimensionless parameters are the ratio of specific heats γ , a kinetic parameter κ , the heat of reaction q , and the activation energy Θ . Here the substantial derivative $\frac{d}{dt} = \frac{\partial}{\partial t} + v_i \frac{\partial}{\partial x_i}$

Equations (1–3) express conservation principles for mass, momenta, and energy, respectively. Equation (4) is a species evolution equation which incorporates an Arrhenius depletion model. Equations (5–6) are caloric and thermal equations of state. A single, first-order, irreversible, exothermic reaction is employed, $A \rightarrow B$. The reaction progress variable λ ranges from zero before reaction to unity at complete reaction. Species mass fractions, Y_i are related to the reaction progress variable by the formulæ, $Y_A = 1 - \lambda$, $Y_B = \lambda$. Initial pre-shock conditions are specified as $\rho = 1$, $u = \sqrt{\gamma} M_0$, $v = 0$, $P = 1$, $T = 1$, $e = 1/(\gamma - 1)$, and $\lambda = 0$. Here M_0 is the freestream Mach number.

In Eqs. (1-6) pressure, density, and temperature are scaled so their pre-shock values are unity; velocities are scaled by a number closely related to the pre-shock acoustic speed. The length of the projectile (\tilde{L}) is chosen as the reference length scale. In terms of dimensional (indicated by the notation “~”) variables, parameters, and pre-shock ambient conditions (indicated by the subscript “0”), the dimensionless variables are defined by

$$\begin{aligned} \rho &= \frac{\tilde{\rho}}{\tilde{\rho}_0}, & P &= \frac{\tilde{P}}{\tilde{P}_0}, & T &= \frac{\tilde{R}}{\tilde{P}_0/\tilde{\rho}_0} \tilde{T}, \\ u &= \frac{\tilde{u}}{\sqrt{\tilde{P}_0/\tilde{\rho}_0}}, & v &= \frac{\tilde{v}}{\sqrt{\tilde{P}_0/\tilde{\rho}_0}}, & e &= \frac{\tilde{e}}{\tilde{P}_0/\tilde{\rho}_0}, \\ x &= \frac{\tilde{x}}{\tilde{L}}, & y &= \frac{\tilde{y}}{\tilde{L}}, & t &= \frac{\sqrt{\tilde{P}_0/\tilde{\rho}_0}}{\tilde{L}} \tilde{t}. \end{aligned} \quad (7)$$

The dimensionless parameters are defined by the following relations:

$$\begin{aligned} q &= \frac{\tilde{q}}{\tilde{P}_0/\tilde{\rho}_0}, & \Theta &= \frac{\tilde{E}}{\tilde{P}_0/\tilde{\rho}_0}, & \gamma &= 1 + \frac{\tilde{R}}{\tilde{c}_v}, \\ \kappa &= \frac{\tilde{L}}{\sqrt{\tilde{P}_0/\tilde{\rho}_0}} \tilde{\kappa}, & M_0 &= \frac{\tilde{u}_0}{\sqrt{\gamma \tilde{P}_0/\tilde{\rho}_0}}. \end{aligned} \quad (8)$$

Here the dimensional parameters are \tilde{q} the heat of reaction, \tilde{E} the activation energy, \tilde{R} the gas constant for the particular fluid, \tilde{c}_v the specific heat at constant volume, and \tilde{k} the kinetic rate constant.

Rankine-Hugoniot Jump Analysis

In this section a simple analysis is summarized which can give qualitative predictions for solution properties of Eqs. (1–6).

Jump Relations

A series of jump relations can be developed from Eqs. (1-6) to determine the pressure on each surface as a function of M_0 . Here, we take the high activation energy limit, $\Theta \gg 1$, so that it is proper to describe the entire combustion process as a thin flame sheet and choose kinetic parameters Θ , κ , and q such that estimates from thermal explosion theory place the flame sheet on the lee wedge surface. Consequently, it is possible to use standard relations¹⁸ for inert oblique shocks and centered Prandtl-Meyer expansions to determine the pressure in Regions 1, 2, and 3. For the oblique shock between Regions 0 and 1, the weak solution branch is chosen so as to match to a Mach wave at distances far from the projectile. The flow expands in a Prandtl-Meyer expansion from Region 1 through Region 2 until the flow velocity is parallel to the lee wedge surface in Region 3. With the *ad hoc* assumption that the flame sheet is perpendicular to the wedge surface, a *RH* relation with heat release gives the pressure in Region 4. The deflagration solution branch is chosen here. Though not important in determining the net force, it is also possible to choose an oblique shock location such that the flow in Region 5 is in the x direction only.

Thermal Explosion Theory

Thermal explosion theory provides an estimate for the flame sheet location. With the assumption of chemical reaction occurring in a fixed volume, well-stirred reactor with zero fluid velocity, Equations (1-6) are suitable to determine a time when the reaction rate becomes unbounded. This induction time is a function of the shocked fluid state and kinetic parameters. The shocked fluid velocity is used to associate an induction distance with the induction time. The flame sheet is fixed at this induction distance, which is measured along the wedge surface.

With the assumption of a static fluid, $v_i = 0$, Eq. (1) holds that the fluid is incompressible, and Eq. (2) holds that P is at most $P(t)$. Using the state

relation (6), the system reduces to two equations in P and λ :

$$\frac{dP}{dt} = (\gamma - 1)\rho\kappa q(1 - \lambda) \exp\left(\frac{-\Theta\rho}{P}\right) \quad (9)$$

$$\frac{d\lambda}{dt} = \kappa(1 - \lambda) \exp\left(\frac{-\Theta\rho}{P}\right), \quad (10)$$

$$P(0) = P_1, \quad \lambda(0) = 0.$$

Here, the initial condition on pressure is given by the shock pressure, and the reaction progress is initially zero. These equations can be linearized by assuming $P = P_1 + P'$, $\lambda = \lambda'$, where the primed quantities are relatively small. Using the initial condition $P'(0) = 0$, the linearized equation can be solved exactly for the pressure perturbation P' :

$$P' = -P_1 \frac{P_1/\rho_1}{\Theta} \times \ln \left[1 - \frac{\Theta\rho_1^2}{P_1^2} (\gamma - 1) q\kappa \left(\exp \frac{-\Theta\rho_1}{P_1} \right) t \right]. \quad (11)$$

The pressure perturbation becomes unbounded as the argument of the logarithm approaches zero. This condition fixes a time, t_{ind} , when the reaction rate becomes $O(1)$ and gives rise to a thermal explosion. The induction time and length, L_{ind} , are given by

$$t_{ind} = \frac{P_1^2}{(\gamma - 1)\Theta\rho_1^2 q\kappa} \exp\left(\frac{\Theta\rho_1}{P_1}\right) \quad (12)$$

$$L_{ind} = t_{ind} \sqrt{u_1^2 + v_1^2}, \quad (13)$$

where u_1 and v_1 are the x and y components of velocity behind the lead shock, respectively. It is deduced from Eq. (12) that increasing M_0 typically decreases t_{ind} . This is seen by first noting that the shocked temperature $T_1 = P_1/\rho_1$ and using the result that increasing M_0 increases T_1 . Because for a wide variety of cases it can be shown that increasing T_1 decreases the exponential term faster than it raises the algebraic term, the tendency is for t_{ind} to decrease.

Numerical Analysis

A numerical analysis of Eqs. (1–6) was performed with the RPLUS code¹⁹, obtained from the NASA Lewis Research Center, using standard available features. In brief the code uses a finite volume method that is based on the lower-upper symmetric successive overrelaxation (LU-SSOR) implicit factorization scheme. Given an initial condition, the code, with

artificially large time steps, solves Eqs. (1–6) recursively until the unsteady terms have relaxed to a preset number near zero, yielding a candidate steady solution. In the version used for the present study, the spatial discretization is achieved with central differencing. To minimize the amplitude of oscillations near shocks, a combined second-order and fourth-order artificial dissipation term is used. A common 199×99 fixed grid was used to model all cases. All cases were run on an IBM RS/6000 POWERstation 350 with a speed of 18.6 Mflops and 64 Mb RAM. The cases were cycled through 500 iterations at which point the residual unsteady terms had a scaled value of less than 1×10^{-8} . Each case required little over one hour to converge at this level.

Results

We look for steady propagation speeds which give rise to a force balance as the heat release parameter q is varied, $15.657 \leq q \leq 20.6$. Other parameters are held constant at $\gamma = 7/5$, $\theta = 5^\circ$, $\Theta = 12.32$, and $\kappa = 3,477$. For presentation of dimensional results we take corresponding dimensional values to be $\tilde{P}_0 = 1.01325 \times 10^5$ Pa, $\tilde{\rho}_0 = 1.225$ kg/m³, $\tilde{k} = 1 \times 10^7$ s⁻¹, $\tilde{E} = 1.019 \times 10^6$ J/kg, $\tilde{L} = 0.1$ m, $\tilde{R} = 287$ J/(kgK), $\tilde{c}_v = 717.5$ J/(kgK), 1.295×10^6 J/kg $\leq \tilde{q} \leq 1.704 \times 10^6$ J/kg. These values were chosen not so much to model a real system but so that the method could be successfully illustrated and an interesting bifurcation phenomenon predicted. For models which better represent physical systems, it is certain that the method given here can be applied and plausible that the predictions will have the same essence.

The projectile will have a steady velocity when the force due to pressure wave drag which tends to retard the motion is balanced by forces induced by combustion which tend to accelerate the projectile. The dimensionless net force per unit depth F_i is given by the pressure force integrated over the circumference C of the diamond-shaped wedge:

$$F_i = \int_C P n_i ds \quad (14)$$

where ds is an element of arc length of the diamond-shaped wedge of Fig. 3. Due to symmetry, the only non-zero component of F_i is in the x direction. This force, named F_{net} , is defined to be positive if it points in the negative x direction. For the *RH* analysis it is given by

$$F_{net} = \tan\theta [P_3(2L_{ind} \cos\theta - 1) + P_4(2 - 2L_{ind} \cos\theta) - P_1]. \quad (15)$$

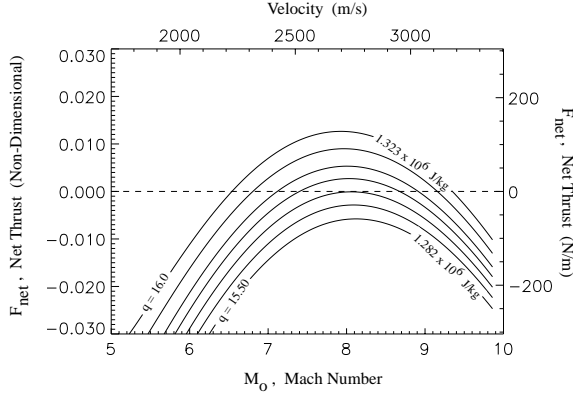


Figure 5: Net thrust force vs. Mach number, varying heat release, *RH* analysis.

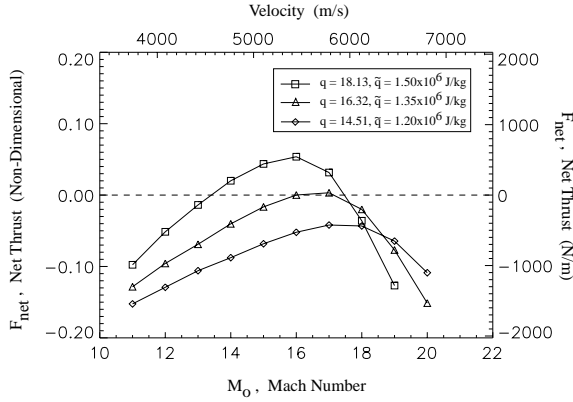


Figure 6: Net thrust force versus Mach number, varying heat release, numerical.

Figure 5 shows F_{net} versus M_0 for seven values of q . For the numerical analysis, numerical integration of the pressure field gives the net thrust. Figure 6 is the equivalent of Fig. 5 for the numerical analysis. Here F_{net} is plotted vs. M_0 for the three indicated values of q .

Similar trends are evident in both the *RH* and numerical results. For low heat release the net thrust force is negative; the thrust force induced by combustion is not sufficient to overcome the wave drag. At a critical value of heat release, $q = 15.657$ for *RH* analysis and $q = 16.2$ for numerical analysis, there is a balance of combustion-induced thrust and drag such that the net thrust is zero. This occurs at $M_0 = 8.05$ in the *RH* analysis and at a significantly higher number, $M_0 = 16.5$, for the numerical analysis. As heat release continues to increase, there are two distinct Mach numbers for which there is no net thrust. A perturbation in the Mach number for the steady solution at the lower Mach number results in

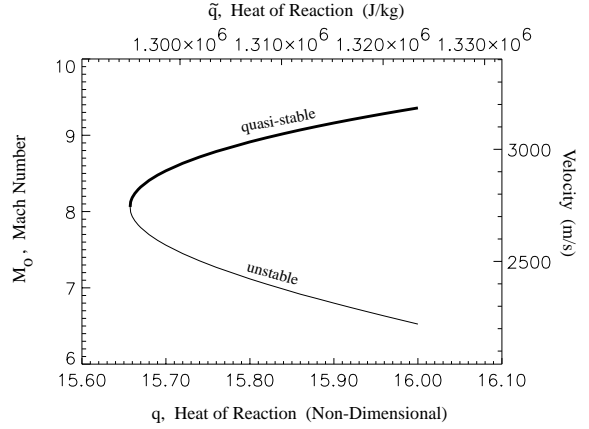


Figure 7: Bifurcation diagram for steady state speed versus heat of reaction, *RH* analysis.

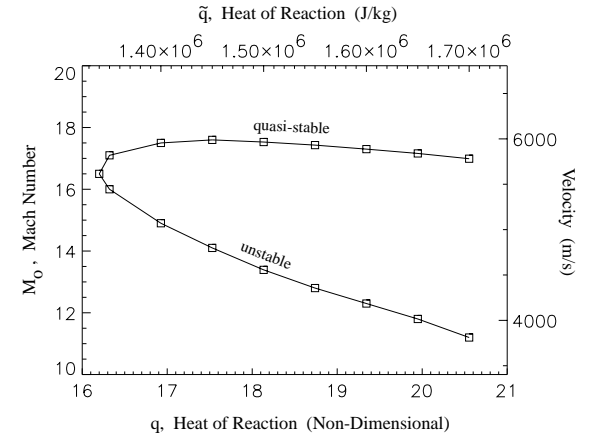


Figure 8: Bifurcation diagram for steady state speed versus heat of reaction, numerical analysis.

a perturbed net force which tends to accelerate the projectile away from the equilibrium Mach number. Consequently, this is an unstable equilibrium. In the same manner, it is easily seen that the equilibrium solution at the higher Mach number is quasi-stable to such perturbations. As heat release is increased, the quasi-stable, high Mach number solution's Mach number increases and the flame sheet is located closer to the expansion fan, while the unstable, low Mach number solution's Mach number decreases and the flame sheet is located closer to the trailing edge.

Both the *RH* and numerical results are conveniently summarized in the bifurcation diagrams shown in Figs. 7 and 8, respectively. Here we plot the equilibrium Mach numbers M_0 versus q . The lower branch is unstable while the upper branch is quasi-stable. On the quasi-stable branch near the bifurca-

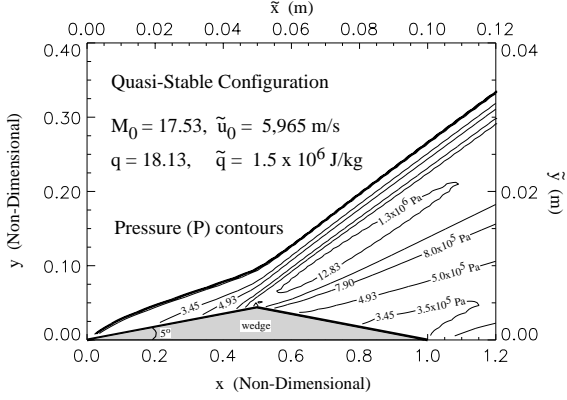


Figure 9: Pressure contours for quasi-stable steady configuration.

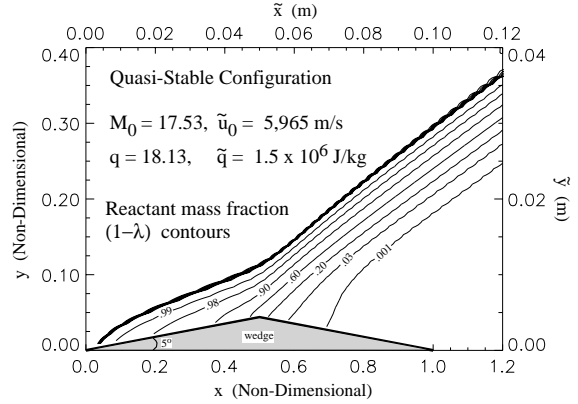


Figure 10: Reactant mass fraction contours for quasi-stable configuration.

tion point, an increase in q causes the flight speed to increase. For the *RH* results, the solutions shown correspond to quasi-stable flight speeds in the range of $2,739 \text{ m/s} \leq \tilde{u}_0 \leq \sim 3,200 \text{ m/s}$, $8.05 \leq M_0 \leq \sim 9.5$. The equivalent numerical results are for a wider range of q . The solutions shown here correspond to quasi-stable flight speeds in the range of $\sim 5,500 \text{ m/s} \leq \tilde{u}_0 \leq \sim 6,000 \text{ m/s}$, $\sim 16.2 \leq M_0 \leq \sim 18$. As for the *RH* predictions, near the bifurcation point, an increase in q causes the flight speed to rise initially. However, past a critical q , here near $q = 18$, the quasi-stable flight speed begins to decrease. Examination of the results indicates that significant reaction is beginning to occur on the front side of the wedge.

For a particular value of heat release, $q = 18.13$ ($\tilde{q} = 1.5 \times 10^6 \text{ J/kg}$), detailed plots of pressure contours and reactant mass fraction ($1 - \lambda$) contours are given for the quasi-stable case ($M_0 = 17.53$) and the unstable case ($M_0 = 13.4$) in Figs. 9, 10, 11, 12, respectively. The pressure along the curve which begins on the axis of symmetry at the left grid boundary, traces along the projectile surface, and then along the axis of symmetry to the right boundary is plotted in Fig. 13 for these cases.

In the quasi-stable configuration, the lead oblique shock undergoes a sudden increase in angle of inclination from $\sim 11^\circ$ to $\sim 18^\circ$. A similar rise from $\sim 11^\circ$ to $\sim 24^\circ$ occurs for the unstable case. This appears to be associated with the chemical reaction. The reaction occurs sooner for the quasi-stable case which is at the higher Mach number. In both, there is some reaction on the front side of the wedge and significant reaction within the rarefaction zone which prevents freezing the reaction.

As seen in Fig. 13, the pressure varies significantly

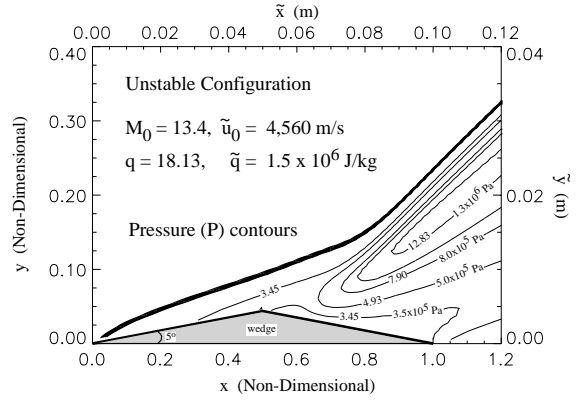


Figure 11: Pressure contours for unstable steady configuration.

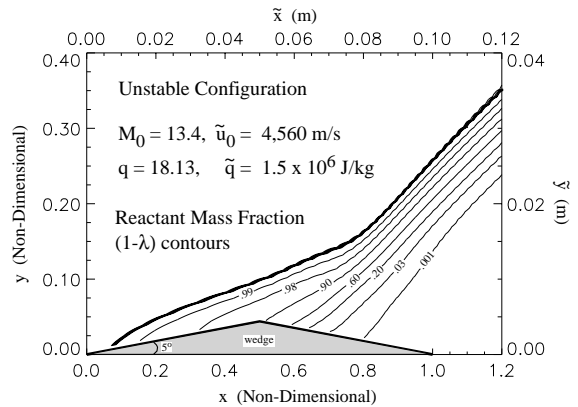


Figure 12: Reactant mass fraction contours for unstable steady configuration.

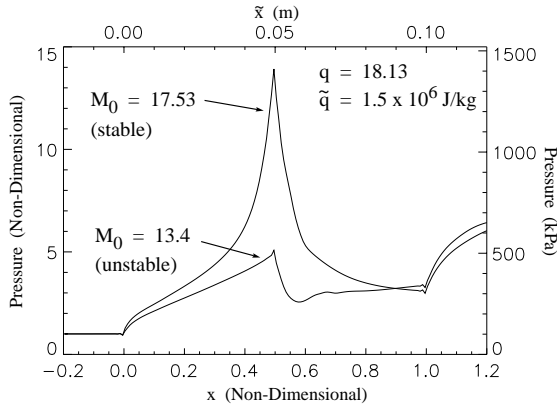


Figure 13: Pressure traces on wedge surface.

on the wedge surface. Here there are about 124 grid points evenly distributed on the wedge surface. For both cases there is a relatively smooth rise on the forebody from the ambient state to a peak value near the apex. The pressures generally fall from here until the downstream oblique shock is encountered at the tail of the projectile.

There seems to be evidence of significant uncertainty associated with these pressures. We believe it is attributable to a lack of numerical resolution. First they are not entirely consistent with the studies of Refs. 13 and 16 which considered an identical model. With both asymptotic and highly resolved numerical solutions from the same code for only the wedge forebody, these papers have shown that the pressure on the wedge surface increases sharply at the wedge tip, continues to rise to a maximum value, and then decreases slightly. Also, comparisons with inert oblique shock predictions suggest a more refined solution is necessary. For $M_0 = 17.53$, the inert shock angle is 7.46° ; the post-shock pressure is $P_1 = 5.87$. For $M_0 = 13.4$, the shock angle is 8.26° ; the post-shock pressure is $P_1 = 4.16$. It is noted that the numerical value of the steady propagation speed is highly sensitive to the pressure. Because of the present uncertainties, the results are best taken as qualitative only.

Finally, it is noted that in the far-field limit, the oblique shock should relax to a Mach wave with insufficient strength to ignite the mixture. Apparently the domain is not sufficiently large to capture this, though it should not affect the pressure distribution on the wedge surface.

Conclusions

This study has given indication of the importance

of the interaction of kinetic length scales with geometric length scales in determining steady propagation velocities for high Mach number propulsion devices. The trends of our variation of net thrust with Mach number for fixed heat release are consistent with those of Refs. 1 and 2. Most importantly, the idea of using the heat release to vary the propagation speed, as shown in the bifurcation diagrams, has been demonstrated. In an ODWE environment, the equivalence ratio could presumably be varied to achieve this effect. Alternatively, one may be able to use the wedge angle as a bifurcation parameter to vary the propagation speed.

For the future, it may be possible to develop a thin airfoil theory to more firmly ground the asymptotic results. It should also be possible to use an adaptive grid with higher resolution to improve the numerical accuracy.

References

- ¹Brackett, D. C., and Bogdanoff, D. W., "Computational investigation of oblique detonation ramjet-in-tube concepts," *Journal of Propulsion and Power*, Vol. 5, No. 3, 1989, pp. 276-281.
- ²Yungster, S., and Bruckner, A. P., "Computational studies of a superdetonative ram accelerator mode," *Journal of Propulsion and Power*, Vol. 8, No. 2, 1992, pp. 457-463.
- ³Powers, J. M., and Gonthier, K. A., "Methodology and Analysis for Determination of Propagation Speed of High-Speed Propulsion Devices," Proceedings of the Central States Section Spring 1992 Technical Meeting of the Combustion Institute, April 1992, pp. 1-6.
- ⁴Hertzberg, A., Bruckner, A. P., and Bogdanoff, D. W., "Ram Accelerator: A New Chemical Method for Accelerating Projectiles to Ultrahigh Velocities," *AIAA Journal*, Vol. 26, No. 2, 1988, pp. 195-203.
- ⁵Hertzberg, A., Bruckner, A. P., and Knowlan, C., "Experimental Investigation of Ram Accelerator Propulsion Modes," *Shock Waves*, Vol. 1, 1991, pp. 17-25.
- ⁶Dunlap, R., Brehm, R. L., and Nicholls, J. A., "A preliminary study of the application of steady-state detonative combustion to a reaction engine," *Jet Propulsion*, Vol. 28, No. 7, 1958, pp. 451-456.
- ⁷Cambier, J. L., Adelman, H., and Menees, G. P., "Numerical Simulations of Oblique Detonations in Supersonic Combustion Chambers," *Journal of Propulsion and Power*, Vol. 5, No. 4, 1989, pp. 483-491.
- ⁸Cambier, J. L., Adelman, H., and Menees, G. P., "Numerical Simulations of an Oblique Detona-

tion Wave Engine," *Journal of Propulsion and Power*, Vol. 6, No. 3, 1990, pp. 315-323.

⁹Yungster, S., Eberhardt, S., and Bruckner, A. P., "Numerical simulation of hypervelocity projectiles in detonable gases," *AIAA Journal*, Vol. 29, No. 2, 1991, pp. 187-199.

¹⁰Bruckner, A. P., Knowlen, C., Hertzberg, A., and Bogdanoff, D. W., "Operational characteristics of the thermally choked ram accelerator," *Journal of Propulsion and Power*, Vol. 7, No. 5, 1991, pp. 828-836.

¹¹Pratt, D. T., Humphrey, J. W., and Glenn, D. E., "Morphology of Standing Oblique Detonation Waves," *Journal of Propulsion and Power*, Vol. 7, No. 5, 1991, pp. 837-845.

¹²Bogdanoff, D. W., "Ram accelerator direct space launch system: new concepts," *Journal of Propulsion and Power*, Vol. 8, No. 2, 1992, pp. 481-490.

¹³Powers, J. M., and Stewart, D. S., "Approximate Solutions for Oblique Detonations in the Hypersonic Limit," *AIAA Journal*, Vol. 30, No. 3, 1992, pp. 726-736.

¹⁴Powers, J. M., and Gonthier, K. A., "Reaction Zone Structure for Strong, Weak Overdriven, and Weak Underdriven Oblique Detonations," *Physics of Fluids A*, Vol. 4, No. 9, 1992, pp. 2082-2089.

¹⁵Yungster, S., "Numerical study of shock-wave/boundary-layer interactions in premixed combustible gases," *AIAA Journal*, Vol. 30, No. 10, 1992, pp. 2379-2387.

¹⁶Grismer, M. J., and Powers, J. M., "Comparisons of Numerical Numerical Oblique Detonation Solutions with an Asymptotic Benchmark," *AIAA Journal*, Vol. 30, No. 12, 1992, pp. 2985-2987.

¹⁷Pepper, D. W., and Brueckner, F. P., "Simulation of an oblique detonation wave scramaccelerator for hypervelocity launchers," in *Computers and Computing in Heat Transfer Science and Engineering*, W. Nakayama and K. T. Yang, eds., CRC Press, Boca Raton, Florida, 1993, pp. 119-137.

¹⁸Shapiro, A. H., *The Dynamics and Thermodynamics of Compressible Fluid Flow, Volume I*, John Wiley, New York, 1953.

¹⁹Shuen, J.-S., and Yoon, S., "Numerical Study of Chemically Reacting Flows Using a Lower-Upper Symmetric Successive Overrelaxation Scheme," *AIAA Journal*, Vol. 27, No. 12, 1989, pp. 1752-1760.